Catalysis Communications 97 (2017) 111–115

Contents lists available at ScienceDirect

Catalysis Communications

journal homepage: www.elsevier.com/locate/catcom

Short communication

Iron-niobium composite oxides for selective catalytic reduction of NO with NH_3

Nana Zhang[a], Ying Xin[a], Xiao Wang[a], Mingfen Shao[a], Qian Li[a], Xicheng Ma[b], Yongxin Qi[c], Lirong Zheng[d], Zhaoliang Zhang[a,*]

[a] School of Chemistry and Chemical Engineering, Shandong Provincial Key Laboratory of Fluorine Chemistry and Chemical Materials, University of Jinan, Jinan 250022, China
[b] School of Chemistry and Chemical Engineering, Shandong University, Jinan 250100, China
[c] School of Material Science and Technology, Shandong University, Jinan 250100, China
[d] Institute of High Energy Physics, Chinese Academy of Sciences, Beijing 100049, China

ARTICLE INFO

Keywords:
Iron-niobium composite oxides
Nitrogen oxides
Selective catalytic reduction
Redox property
Acidity

ABSTRACT

Iron-niobium composite oxides (Nb_aFeO_x, *a* represents the mass percent of Nb in Fe-Nb composite oxides) were studied for the selective catalytic reduction (SCR) of NO_x with NH_3. The Nb-doped Fe_2O_3 was found to be responsible for the improved activity. The doping of Nb into Fe_2O_3 resulted in the improvement of specific surface areas, redox property and acidic amount. The optimal $Nb_{30.3}FeO_x$ sample exhibited nearly 100% NO_x conversion and N_2 selectivity from 250 °C to 400 °C, which would be a promising candidate for NH_3-SCR catalysts in the medium temperature ranges.

1. Introduction

Nitrogen oxides (NO_x) are main air pollutants causing photochemical smog, acid rain, ozone depletion, and greenhouse effects [1]. Among various NO_x control technologies, selective catalytic reduction of NO_x with NH_3 (NH_3-SCR) has been demonstrated as the most efficient one in the after-treatment process. Nowadays, the most widely used NH_3-SCR catalyst is V_2O_5-WO_3/TiO_2 [2,3], however some unavoidable disadvantages still remained, such as the toxicity of vanadium species, the poor activity at temperatures lower than 350 °C and the high oxidation of NH_3 at the high temperature [4,5]. Consequently, the exploration of the novel eco-friendly SCR catalysts with high activity and N_2 selectivity over wide-temperature ranges is never stopped.

It is well known that the excellent redox capability and acidity of catalysts are favorable to the NH_3-SCR reaction [6]. Thus, transition metal oxides with prominent redox property are considered to be the promising candidates for NH_3-SCR catalysts [7,8]. Therein, iron oxides (typically Fe_2O_3) have been received considerable attention because of their non-toxicity and abundance [9–11]. Nevertheless, pure Fe_2O_3 often suffers from poor activity at the low temperature [12]. Therefore, many researchers tried to introduce hetero atoms into Fe_2O_3 to improve the properties and consequently the catalytic activity, for example, Fe-Ti [13], Fe-Ce [14], and Fe-Mn composite oxides, etc. [15,16].

Generally, niobium oxides have gained attention as catalysts due to the high acidity [17]. As early as in 1985, Okazaki et al. first reported the promotion effect of Nb_2O_5 to Fe_2O_3 catalyst for NH_3-SCR reaction [18]. However, the characteristic details were lost in the long history. Afterwards, Vikulov et al. found similar results in Nb_2O_5-modified V_2O_5/TiO_2 [19]. Lian et al. showed that the addition of Nb to MnO_x enhanced the acidity, especially the Brønsted acidity, which brought about the low temperature SCR activity [20]. While Ding et al. reported that the introduction of Nb into $CeZr_2O_x$ allows for a high surface area, the strong surface acidity and redox ability, all of which are beneficial to the remarkable SCR performance [21].

Herein, a series of Fe-Nb composite oxides were synthesized and characterized in depth. X-ray diffraction (XRD) showed the presence of the Nb-doped Fe_2O_3 and $FeNbO_4$ phases in Fe-Nb composite oxides. However, only was the Nb-doped Fe_2O_3 found to be responsible for the improved activity in NH_3-SCR. The doping of Nb into Fe_2O_3 resulted in the improvement of specific surface areas, redox property and acidic amount, which gained the maximum at 30.3 wt% Nb. $Nb_{30.3}FeO_x$ exhibited nearly 100% NO_x conversion and N_2 selectivity from 250 °C to 400 °C, demonstrating a promising candidate for the SCR catalysts in the medium temperature range.

* Corresponding author.
E-mail address: chm_zhangzl@ujn.edu.cn (Z. Zhang).

http://dx.doi.org/10.1016/j.catcom.2017.04.033
Received 9 January 2017; Received in revised form 7 March 2017; Accepted 17 April 2017
Available online 18 April 2017
1566-7367/

2. Experimental section

2.1. Sample preparation

The Fe-Nb composite oxides were prepared by a co-precipitation method. In a typical process, a certain amount of $NbCl_5$ was dissolved in 50 mL of deionized water with magnetic stirring at room temperature. Similarly, $FeSO_4{\cdot}7H_2O$ and ascorbic acid (mole ratio is 1:1.1) were dissolved in 100 mL of deionized water and stirred to obtain a clear solution, and then it was dropwise added into the $NbCl_5$ aqueous solution with magnetic stirring for 10 min at room temperature. The total amount of the metallic ions was 0.033 g/mL. Subsequently, the excess urea solution (2 mol/L) was added into the mixed solution and then heated under reflux aging at 90 °C over 12 h. The precipitate was collected by filtration and washing with deionized water, followed by drying at 100 °C overnight and calcinating at 500 °C for 5 h in air. The obtained mixed oxides were denoted as Nb_aFeO_x, where *a* represents the mass percent (wt%) of Nb in Fe-Nb composite oxides based on inductively coupled plasma-atomic emission spectrometry (ICP-AES). For comparison, pure Fe_2O_3 and Nb_2O_5 were synthesized by the same procedure, while $FeNbO_4$ was prepared by the solid state reaction [22]. The mechanically mixed sample was obtained by grinding the mixture of Fe_2O_3 and $FeNbO_4$ nanoparticles with the Nb content according to the quantitative XRD analysis of $Nb_{30.3}FeO_x$.

2.2. Characterization

XRD patterns were recorded with a Rigaku D/max 2500PC diffractometer using Cu Kα (= 0.15405 nm) radiation and intensity data were collected over a 2θ range of 10 to 90°. A Micromeritics ASAP2020M instrument was used to measure the N_2 adsorption isotherms of the samples at liquid N_2 temperature (− 196 °C). Before the N_2 physisorption, all the samples were degassed at 300 °C. ICP-AES experiments were carried out on an IRIS Intrepid IIXSP instrument from Thermo Elemental. High-resolution transmission electron microscopy (HRTEM) was conducted on a JEOL JEM-2010 at an accelerating voltage of 200 kV. X-ray absorption fine structure (XAFS) measurements for the Fe K-edge and Nb K-edge were performed in the transmission mode at room temperature on the XAFS station of the 1W1B beamline of Beijing synchrotron radiation facility (BSRF, Beijing, China). H_2 temperature-programmed reduction (H_2-TPR) experiments were carried out on a quartz reactor with a thermal conductivity detector (TCD) to monitor H_2 consumption. The samples (50 mg) in a quartz reactor were pretreated at 500 °C for 30 min in O_2 and cooled down to the room temperature. Then a 50 mL/min gas flow of 5 vol% H_2 in N_2 was passed over the samples with the rate of 10 °C/min up to 800 °C. NH_3-temperature programmed desorption (NH_3-TPD) experiments were performed in a quartz reactor using 50 mg catalyst. Prior to the experiments, the samples (40–60 mesh) in a quartz reactor were pretreated at 500 °C for 30 min in 10 vol% O_2/He (50 mL/min) to remove surface impurities and then cooled to the 30 °C. NH_3 adsorption was operated in 4000 ppm NH_3/He (50 mL/min) until the concentration stabilized. Then the weak adsorbed ammonia was purged with highly pure He. Finally, the samples were heated up to 700 °C at a heating rate of 10 °C/min. NH_3 was detected using quadrupole mass spectrometer (OmniStar 200, Balzers).

2.3. Catalytic performance testing

All samples were tested for SCR activity in a fixed-bed quartz tube reactor (6.0 mm i.d.) with a thermocouple placed inside the catalyst bed and in the temperature range 150–450 °C. The experimental conditions were controlled as follows: 500 ppm NO, 500 ppm NH_3, 5.3% O_2, 100 ppm SO_2 (when used), 5% H_2O (when used) and balance He. The total flow rate was 300 mL/min and the gas hourly space velocity (GHSV) was 50,000 h^{-1}. Concentrations of NO and NO_2 were determined by a chemiluminiscence NO_x analyzer (42*i*-HL, Thermo), in addition, NH_3 and N_2O were detected by using a quadrupole mass spectrometer (MS, OmniStar 200, Balzers) at m/z = 44 for N_2O, and 17 for NH_3. The NO_x conversion and N_2 selectivity were calculated according to the following equation:

$$NO_x \text{ conversion} = \frac{[NO_x]_{inlet} - [NO_x]_{outlet}}{[NO_x]_{inlet}} \times 100\%$$

$$N_2 \text{ selectivity} = \frac{[NO_x]_{inlet} + [NH_3]_{inlet} - [NO_x]_{outlet} - [NH_3]_{outlet} - 2 \times [N_2O]_{outlet}}{[NO_x]_{inlet} + [NH_3]_{inlet} - [NO_x]_{outlet} - [NH_3]_{outlet}} \times 100\%$$

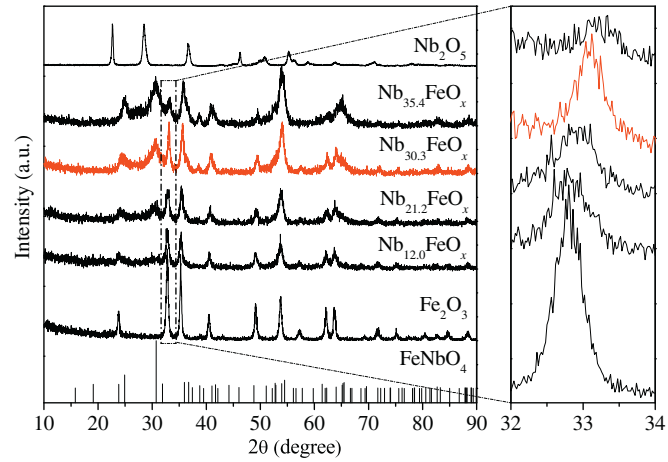

Fig. 1. XRD patterns of Fe_2O_3, Nb_2O_5 and Nb_aFeO_x.

3. Results and discussion

3.1. XRD

Powder XRD was conducted to investigate the crystal structure of Nb_aFeO_x (Fig. 1). Pure iron and niobium oxides are present as Fe_2O_3 (JCPDS 33-0664) and Nb_2O_5 (JCPDS 30-0873), respectively. For $Nb_{12.0}FeO_x$, the XRD peaks are indexed as a hematite phase of Fe_2O_3, while no diffraction peaks of Nb-containing species was detected. Increasing in the Nb content results in the emergence of a new phase $FeNbO_4$ (JCPDS 71-1849) (Fig. S1) as for $Nb_{21.2}FeO_x$, $Nb_{30.3}FeO_x$, and $Nb_{35.4}FeO_x$. Furthermore, compared with pure Fe_2O_3, the peaks of Fe_2O_3 in Nb_aFeO_x shift to the higher angle (inset) deriving from the lattice constriction. The decreased lattice parameter *a* (Table 1) for the Fe_2O_3 phase correspond to the increasing Nb content in Nb_aFeO_x, owing to the substitution of Fe ions (0.0645 nm) by the smaller Nb ions (0.064 nm) [23]. This suggests that a fraction of Nb atoms was doped into the Fe_2O_3 lattice besides the formation of $FeNbO_4$. The relative amount of $FeNbO_4$ in Nb_aFeO_x can be obtained using the quantitative XRD analysis by the reference intensity ratio (RIR) method (Table 1 and Supporting information) [24]. In combination with the ICP data, the doping amount of Nb into the Fe_2O_3 lattice was roughly calculated (Table 1), which corresponded well with lattice parameter *a*. Furthermore, with the doping amount increasing, the crystallinity of hematite is decreased, especially for $Nb_{35.4}FeO_x$.

3.2. N_2 adsorption/desorption and TEM

The surface areas and pore distribution were characterized by N_2 adsorption/desorption (Table 1 and Fig. S2). As shown in Table 1, all Nb_aFeO_x samples possess much higher BET surface areas than those of pure Fe_2O_3 and Nb_2O_5. The largest surface area of 84.7 m^2/g was obtained for $Nb_{30.3}FeO_x$, indicating the optimal doping amount for specific surface areas. N_2 adsorption/desorption isotherms exhibit

Table 1
ICP, XRD, surface area, H_2-TPR and NH_3-TPD data for Fe_2O_3, Nb_2O_5 and Nb_aFeO_x.

Samples	Nb mass percent (wt%)[a]	Nb in $FeNbO_4$ (wt %)[b]	Nb doped into Fe_2O_3 (wt%)	Lattice parameter *a* (Å)	Surface area (m^2/g)	Peak position of H_2-TPR (°C)	Total amount of NH_3 desorption (mmol/g)
Fe_2O_3	–	–	–	5.086	48.1	398	198.9
$Nb_{12.0}$-Fe_2O_3	12.0	–	12.0	5.045	71.1	393	271.1
$Nb_{21.2}$-Fe_2O_3	21.2	6.7	14.5	5.035	73.2	393	287.6
$Nb_{30.3}$-Fe_2O_3	30.3	7.7	22.6	5.030	84.7	380	314.4
$Nb_{35.4}$-Fe_2O_3	35.4	10.8	24.6	5.023	77.3	386	281.6
Nb_2O_5	–	–	–	–	32.6	–	163.0

[a] ICP data.
[b] Obtained from the quantitative XRD analysis.

typical IV curves and H1 type hysteresis loops (Fig. S2a), suggesting the existence of mesopores and a small fraction of macropores (Fig. S2b), which originate from the interstices between the particles.

The morphology and microstructures were further investigated by TEM taking $Nb_{30.3}FeO_x$ as an example (Fig. S3). The nanoparticles of 10–20 nm were aggregated together (Fig. S3a), which can be distinguished as the Nb-doped Fe_2O_3 and $FeNbO_4$ (Fig. S3b), in good agreement with XRD and pore distribution analysis for Nb_aFeO_x.

3.3. XAFS

XAFS can be used to determine the local environment around specific atoms, which may influence the performance of catalysts. Fig. 2 shows the radial structure function (RSF) curves of Fe and Nb K-edge EXAFS spectra for Fe_2O_3, Nb_2O_5, $FeNbO_4$ and Nb_aFeO_x. In Fig. 2a, Fe_2O_3 shows two characteristic peaks assigned to the Fe-O and Fe-O-Fe shells together with an obvious shoulder peak, which was also typical for α-Fe_2O_3 [13]. In the case of Nb_aFeO_x, the coordination environment of iron is similar to that of Fe_2O_3, while the intensity of the shoulder peak is relatively stronger than that of the Fe-O-Fe shell, which is caused by the co-existed $FeNbO_4$. In Fig. 2b, $FeNbO_4$ shows two characteristic peaks, one belongs to Nb-O shell together with an obvious shoulder and the other assigns to Nb-O-Fe shell. For Nb_aFeO_x, the position of the Nb-O-Fe peak shows a slight shift to higher R value in comparison with $FeNbO_4$, suggesting the contribution from the doped Nb species in Fe_2O_3.

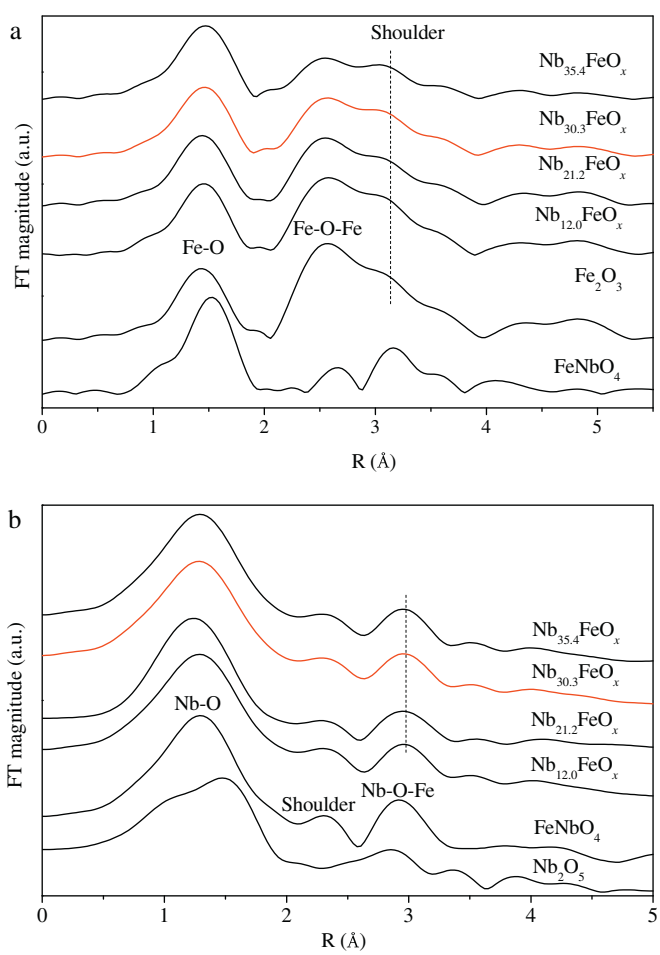

Fig. 2. The radial structure function (RSF) curves of Fe (a) and Nb (b) K-edge EXAFS spectra for Fe_2O_3, Nb_2O_5, $FeNbO_4$ and Nb_aFeO_x.

3.4. H_2-TPR

To study the redox property of the samples, H_2-TPR was performed. Fig. 3 shows the H_2-TPR patterns of Fe_2O_3, Nb_2O_5, $FeNbO_4$ and Nb_aFeO_x. The pristine Fe_2O_3 shows three reduction peaks at 396 °C, 638 °C and > 700 °C, which can be assigned to the reduction of Fe_2O_3 to Fe_3O_4 (396 °C), Fe_3O_4 to FeO (638 °C) and FeO to Fe (> 700 °C), respectively [16,25]. Nb_2O_5 and $FeNbO_4$ do not show obvious reduction peaks below 700 °C. Thus, the low-temperature redox peaks could be attributed to the reduction of Fe species in the Nb-doped Fe_2O_3 phase. It is clear that the addition of Nb can result in the peak shift to lower temperatures. The lowest reduction peak temperature was reached at $Nb_{30.3}FeO_x$ (Table 1), indicating the optimal doping amount for redox ability. After that the reduction peak shifts to the higher temperature.

3.5. NH_3-TPD

NH_3-TPD was carried out to investigate the effect of Nb contents on acidity of the samples. Fig. 4 shows the NH_3-TPD spectra over Fe_2O_3, Nb_2O_5 and Nb_aFeO_x. The corresponding desorption amounts of NH_3 are

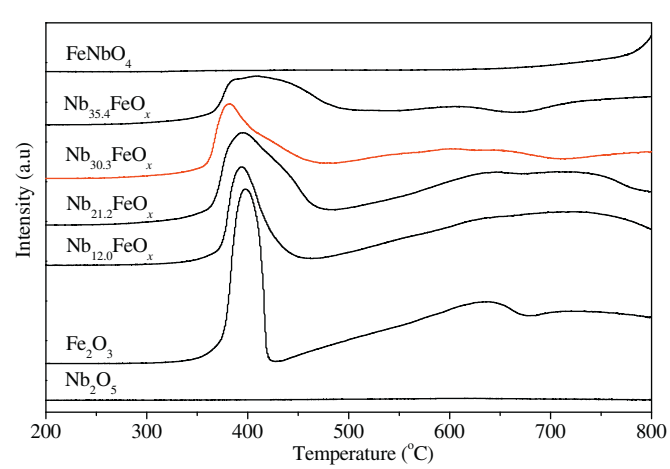

Fig. 3. H_2-TPR profiles of Fe_2O_3, Nb_2O_5, $FeNbO_4$ and Nb_aFeO_x.

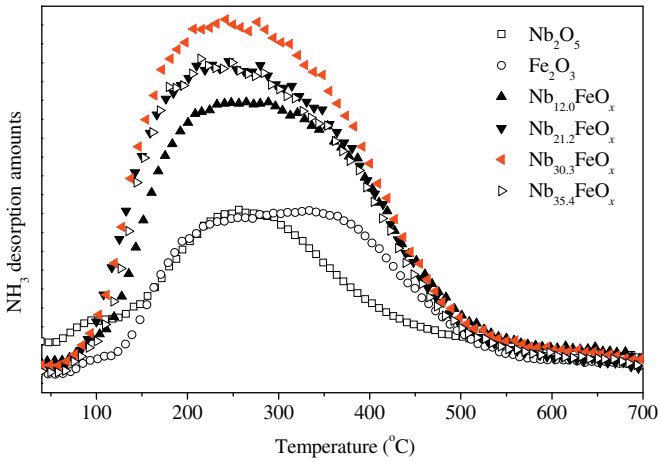

Fig. 4. NH_3-TPD profiles of Fe_2O_3, Nb_2O_5 and Nb_aFeO_x.

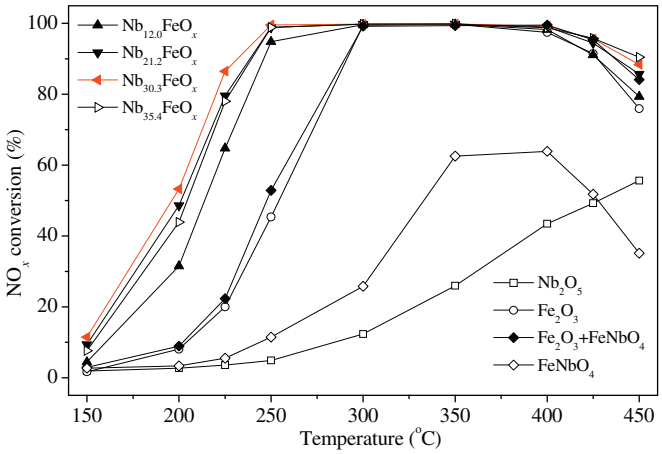

Fig. 5. NO_x conversion in NH_3-SCR as a function of temperature over Fe_2O_3, Nb_2O_5, $FeNbO_4$, Fe_2O_3 + $FeNbO_4$ and Nb_aFeO_x.

listed in Table 1. Both Fe_2O_3 and Nb_2O_5 show broad distributions of NH_3 desorption over a wide temperature range. However, after the addition of Nb, all Nb_aFeO_x samples desorbed much more NH_3 compared with Fe_2O_3. Because $FeNbO_4$ does not show any acidity (not shown here), the promotional effect of acidity is derived from the doping of Nb in Fe_2O_3. Similar to surface areas and redox property, the maximum NH_3 desorption was obtained at $Nb_{30.3}FeO_x$.

3.6. Catalytic performance

NO_x conversion and N_2 selectivity as a function of temperature in NH_3-SCR reactions were shown in Fig. 5 and S4, respectively. In Fig. 5, although both Nb_2O_5 and $FeNbO_4$ are inactive, Fe_2O_3 shows good activity above 300 °C. As expected, all Nb_aFeO_x samples show improved activity at lower temperatures. Because the mixture of Fe_2O_3 and $FeNbO_4$ shows similar activity with that of Fe_2O_3, the improvement of activity for Nb_aFeO_x was attributed to the Nd-doped Fe_2O_3. Among the various samples, $Nb_{30.3}FeO_x$ was optimal and exhibited nearly 100% NO_x conversion and N_2 selectivity from 250 °C to 400 °C at a gas hourly space velocity of 50,000 h^{-1}. In comparison with V_2O_5-WO_3/TiO_2 [26], the temperature widow shifts to lower temperature and the N_2 selectivity is always nearly 100% even at 450 °C (Fig. S4). On the basis of the above characterization results, the high activity over Nb_aFeO_x can be attributed to the high surface area, strong reducibility and large acidic amount due to the doping of Nb in Fe_2O_3.

The stability of Nb_aFeO_x is also considered, taking $Nb_{30.3}FeO_x$ as an example, the catalyst is maintained above 100% NO_x conversion at 250 °C (Fig. S5). Moreover, the resistance to H_2O and SO_2 over $Nb_{30.3}FeO_x$ at 250 °C is checked (Fig. S5). When 5% H_2O and 100 ppm SO_2 were added into the reaction gas, NO_x conversion decreased from 100% to ~80%. However, the initial activity can be recovered after removing SO_2 and heat-treatment of the catalyst at 500 °C.

4. Conclusions

Iron-niobium composite oxides were characterized and studied for NH_3-SCR. XRD, ICP-AES, HRTEM and XAFS show the presence of the Nb-doped Fe_2O_3 and $FeNbO_4$ phases in Fe-Nb composite oxides. However, only is the former responsible for the activity. The doping of Nb into Fe_2O_3 resulted in the improvement of specific surface areas, redox property and acidic amount as detected by N_2 adsorption/desorption, H_2-TPR and NH_3-TPD, respectively. The optimal doping amount was obtained at 30.3 wt% Nb due to the highest surface areas, reducibility and acidic amount. $Nb_{30.3}FeO_x$ exhibits nearly 100% NO_x conversion and N_2 selectivity from 250 °C to 400 °C at a gas hourly space velocity of 50,000 h^{-1}, which demonstrated a promising candidate for the SCR catalysts in the medium temperature ranges.

Acknowledgments

This work was supported by National Natural Science Foundation of China (Nos. 21477046, 21277060, and 21547007), Key Technology R & D Program of Shandong Province (No. 2016ZDJS11A03), and Shandong Provincial Natural Science Foundation, China (No. ZR2016BM32).

Appendix A. Supplementary data

Supplementary data to this article can be found online at http://dx.doi.org/10.1016/j.catcom.2017.04.033.

References

[1] M.A. Gomez-Garcia, V. Pitchon, A. Kiennemann, Pollution by nitrogen oxides: an approach to NO_x abatement by using sorbing catalytic materials, Environ. Int. 31 (2005) 445–467.
[2] G. Busca, L. Lietti, G. Ramis, F. Berti, Chemical and mechanistic aspects of the selective catalytic reduction of NO_x by ammonia over oxide catalysts: a review, Appl. Catal. B Environ. 18 (1998) 1–36.
[3] S. Djerad, L. Tifouti, M. Crocoll, W. Weisweiler, Effect of vanadia and tungsten loadings on the physical and chemical characteristics of V_2O_5-WO_3/TiO_2 catalysts, J. Mol. Catal. A Chem. 208 (2004) 257–265.
[4] Z.P. Qu, L. Miao, H. Wang, Q. Fu, Highly dispersed Fe_2O_3 on carbon nanotubes for low temperature selective catalytic reduction of NO with NH_3, Chem. Commun. 51 (2015) 956–958.
[5] P. Forzatti, Present status and perspectives in de-NO_x SCR catalysis, Appl. Catal. A Gen. 222 (2001) 221–236.
[6] N.Y. Topsøe, Mechanism of the selective catalytic reduction of nitric oxide by ammonia elucidated by in situ on-line fourier transform infrared spectroscopy, Science 265 (1994) 1217–1219.
[7] J.H. Li, H.Z. Chang, L. Ma, J.M. Hao, R.T. Yang, Low-temperature selective catalytic reduction of NO_x with NH_3 over metal oxide and zeolite catalysts-a review, Catal. Today 175 (2011) 147–156.
[8] H. Hu, S.X. Cai, H.R. Li, L. Huang, L.Y. Shi, D.S. Zhang, Mechanistic aspects of deNO_x processing over TiO_2 supported Co-Mn oxide catalysts: structure-activity relationships and in situ DRIFTs analysis, ACS Catal. 5 (2015) 6069–6077.
[9] H. Arai, M. Machida, Removal of NO_x through sorption-desorption cycles over metal oxides and zeolites, Catal. Today 22 (1994) 97–109.
[10] C. Bolm, J. Legros, J.L. Paih, L. Zani, Iron-catalyzed reactions in organic synthesis, Chem. Rev. 104 (2004) 6217–6254.
[11] Y. Li, Y. Wan, Y.P. Li, S.H. Zhan, Q.X. Guan, Y. Tian, Low-temperature selective catalytic reduction of NO with NH_3 over Mn_2O_3-doped Fe_2O_3 hexagonal microsheets, ACS Appl. Mater. Interfaces 8 (2016) 5224–5233.
[12] S.J. Yang, C.X. Liu, H.Z. Chang, L. Ma, Z. Qu, N.Q. Yan, C.Z. Wang, J.H. Li, Improvement of the activity of γ-Fe_2O_3 for the selective catalytic reduction of NO with NH_3 at high temperatures: NO reduction versus NH_3 oxidization, Ind. Eng. Chem. Res. 52 (2013) 5601–5610.
[13] F.D. Liu, H. He, C.B. Zhang, Z.C. Feng, L.R. Zheng, Y.N. Xie, T.D. Hu, Selective catalytic reduction of NO with NH_3 over iron titanate catalyst: catalytic performance and characterization, Appl. Catal. B Environ. 96 (2010) 408–420.

[14] J. Han, J. Meeprasert, P. Maitarad, S. Nammuangruk, L.Y. Shi, D.S. Zhang, Investigation of the facet-dependent catalytic performance of Fe_2O_3/CeO_2 for the selective catalytic reduction of NO with NH_3, J. Phys. Chem. C 120 (2016) 1523–1533.
[15] H.X. Jiang, L. Zhang, J. Zhao, Y.H. Li, M.H. Zhang, Study on MnO_x-FeO_y composite oxide catalysts prepared by supercritical antisolvent process for low-temperature selective catalytic reduction of NO_x, J. Mater. Res. 31 (2016) 702–712.
[16] Z.H. Chen, F.R. Wang, H. Li, Q. Yang, L.F. Wang, X.H. Li, Low-temperature selective catalytic reduction of NO_x with NH_3 over Fe-Mn mixed-oxide catalysts containing $Fe_3Mn_3O_8$ phase, Ind. Eng. Chem. Res. 51 (2012) 202–212.
[17] K. Tanabe, Catalytic application of niobium compounds, Catal. Today 78 (2003) 65–77.
[18] S. Okazaki, H. Kuroha, T. Okuyama, Effect of Nb_2O_5 addition on the catalytic activity of FeO_x for reduction of NO_x with NH_3 and O_2, Chem. Lett. 14 (1985) 45–48.
[19] K.A. Vikulov, A. Andreini, E.K. Poels, A. Bliek, Selective catalytic reduction of NO with NH_3 over Nb_2O_5-promoted V_2O_5/TiO_2 catalysts, Catal. Lett. 25 (1994) 49–54.
[20] Z.H. Lian, F.D. Liu, H. He, X.Y. Shi, J.S. Mo, Z.B. Wu, Manganese-niobium mixed oxide catalyst for the selective catalytic reduction of NO_x with NH_3 at low temperatures, Chem. Eng. J. 250 (2014) 390–398.
[21] S.P. Ding, F.D. Liu, X.Y. Shi, H. He, Promotional effect of Nb additive on the activity and hydrothermal stability for the selective catalytic reduction of NO_x with NH_3 over $CeZrO_x$ catalyst, Appl. Catal. B Environ. 180 (2016) 766–774.
[22] S. Ananta, P. Brydson, N.W. Thomas, Synthesis, formation and characterisation of $FeNbO_4$ powders, J. Eur. Ceram. Soc. 19 (1999) 489–496.
[23] T. Baba, T. Takizawa, K. Harada, H. Yamada, T. Ishihara, A. Takami, Effect of Pr doping on catalytic properties of oxide ion conductor, Zr-Nd-O, for soot oxidation, Catal. Today 251 (2015) 2–6.
[24] F.H. Chung, Quantitative interpretation of X-ray diffraction patterns of mixtures. I. matrix-flushing method for quantitative multicomponent analysis, J. Appl. Crystallogr. 7 (1974) 519–525.
[25] K. Sirichaiprasert, A. Luengnaruemitchai, S. Pongstabodee, Selective oxidation of CO to CO_2 over Cu-Ce-Fe-O composite-oxide catalyst in hydrogen feed stream, Int. J. Hydrogen Energy 32 (2007) 915–926.
[26] S. Djerad, M. Crocoll, S. Kureti, L. Tifouti, W. Weisweiler, Effect of oxygen concentration on the NO_x reduction with ammonia over V_2O_5-WO_3/TiO_2 catalyst, Catal. Today 113 (2006) 208–214.